Supporting information for

Direct one-pot synthesis of ordered mesoporous carbons from lignin with metal coordinated self-assembly

Xiaoqi Wang [b], Xiaoning Liu [a], Richard Lee Smith, Jr [c], Yining Liang [a], Xinhua Qi[a, *]

[a] *College of Environmental Science and Engineering, Nankai University, No. 38, Tongyan Road, Jinnan District, Tianjin 300350, China*

[b] *Agro-Environmental Protection Institute, Chinese Academy of Agricultural Sciences, No. 31, Fukang Road, Nankai District, Tianjin 300191, China*

[c] *Graduate School of Environmental Studies, Tohoku University, Aramaki Aza Aoba 6-6-11, Aoba, Sendai 980-8579, Japan*

[*] *Corresponding author. Email: qixinhua@nankai.edu.cn (X. Qi), Tel: 86-22-2350-1117.*

2D HSQC NMR analysis of organosolv walnut shell lignin

Figure S1 provides the side chain region (δC/δH 40-90/2.5-6.0) and aromatic chain region (δC/δH 100-135/5.5-8.5) of the 2DHSQC NMR spectra of the organosolv walnut shell lignin. The main substructures are shown in Figure S1. The HSQC cross-signals of lignin and related carbohydrates were confirmed by comparison with the literature.[1] Table S1 lists the cross signals of the main lignin and related carbohydrates assigned in the HSQC spectrum. The side chain region at δC/δH 40-90/2.5-6.0 of the 2D HSQC NMR was mainly composed of methoxy (δC/δH 55.6/3.73), *β-O-4'* (A) aryl ether linkages and *β-β'* (B, Resin alcohol). The δC/δH 59.5-59.7/3.40-3.63 represents the C_γ-H_γ in*β*-O-4' substructure, whereas δC/δH 86.0/4.35 correlations correspond to the signal of acylated *γ*-position of S type *β*-O-4' structure in A structure. The A' and A" configuration correlation signals were relatively weak and could be observed only when the view resolution was enlarged. The *β*-5' structure (C, phenylcoumarol) also exists in WSL which can be found by relative *α* and *β* positions at δC/δH 86.5/5.46 and δC/δH 62.5/3.73, respectively. Relative quantification of the main linkages provided a β-O-4: β-β': β-5 ratio of 0.90:0.07:0.03.

A typical GSH type of WSL can be distinguished through aromatic ring region domain at δC/δH 100-135/5.5-8.0, which is consistent with previous literature.[1, 2] The G units showed correlations of C_2–H_2, C_5–H_5 and C_6–H_6 are at δC/δH 110.9/6.98, 114.9/6.77, and 119.0/6.80, respectively, while the S units showed a prominent signal for the 2, 6 correlation at δC/δH 103.8/6.71. Signals in (δC/δH106.2/7.23 and 7.07) corresponding to $C_{2,6}$–$H_{2,6}$ correlations Cα-oxidized in S units (S′) were present in 2D HSQC spectra. Generally, the $C_{2,6}$–$H_{2,6}$ aromatic correlation for the H units was located at δC/δH127.9/7.19, while the $C_{3,5}$–$H_{3,5}$ correlation of the H

unit overlapped with the C5 position of the G unit and the $C_{3,5}$–$H_{3,5}$ correlation of the p-hydroxy-benzoate substructure. The G: S: H ratio was 0.31: 0.49: 0.2 (Table S2) which means that more phenolic -OH are present for WSL to form micelles than other forms of lignin considered in this work. Additionally, there exists portions of p-hydroxycinnamyl alcohol I_{γ} in WSL, which are able to provide -OH. By GPC analysis, the WSL was determined to have a weight-average (M_w) and number-average (M_n) molecular weight of 4732 and 4083 g mol^{-1}, respectively, with a polydispersity of (PD=M_w/M_n) of 1.16 (Table S2) that can be considered to be narrow.

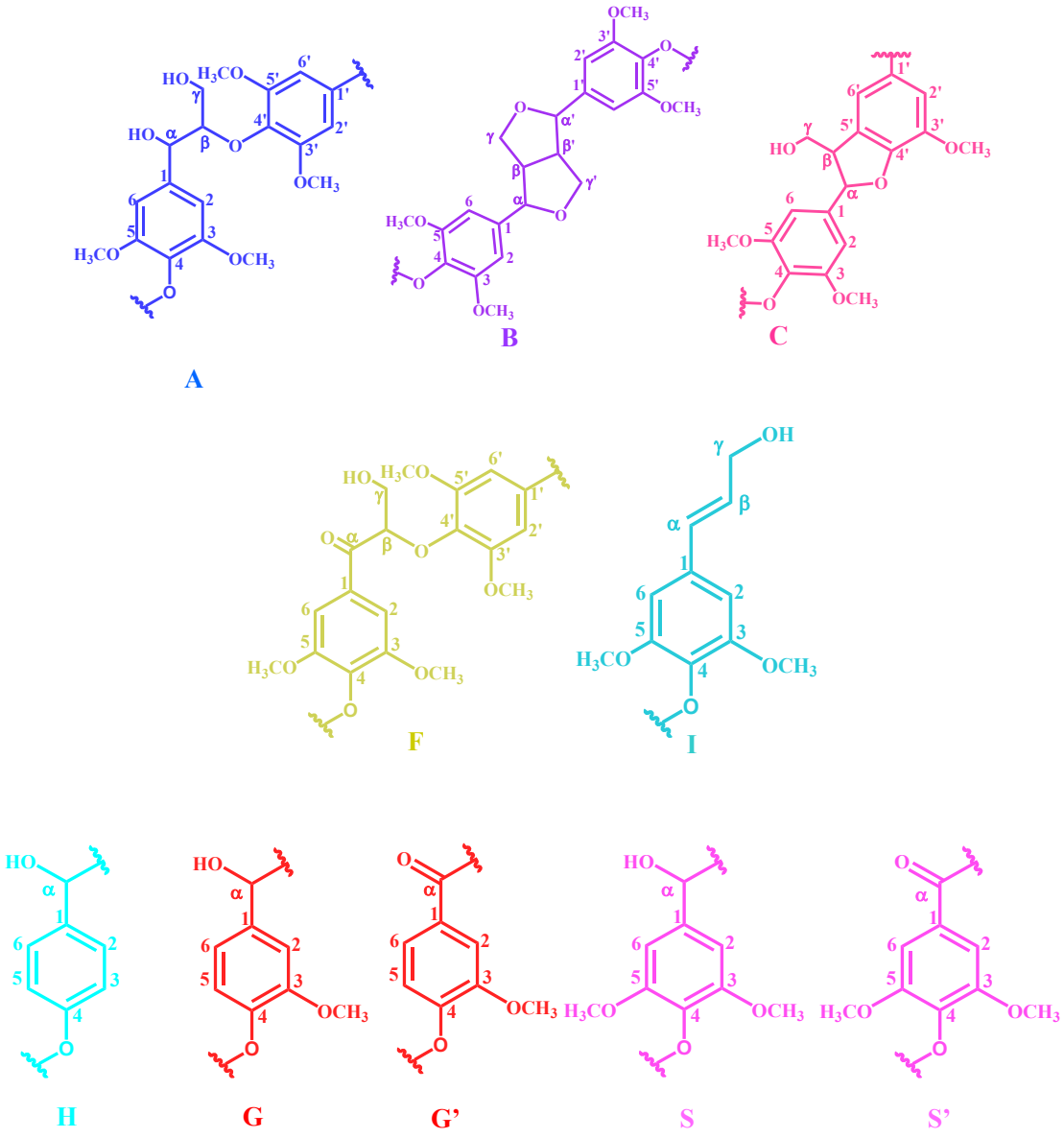

Figure S1. Lignin structures present in WSL: (A) β-O-4' aryl ether linkages with a free -OH at γ-carbon; (B) resinol substructures formed by β-β', α-O-γ', and γ-O-α' linkages; (C) phenyl coumarin substructures formed by β-5' and α-O-4' linkages; (I) p-hydroxycinnamyl alcohol end groups (H) p-hydroxyphenyl units; (G) guaiacyl units; (G') oxidized guaiacyl units with an α-ketone; (S) syringyl units; (S') oxidized syringyl units with a Cα ketone.

Table S1. Assignment of main lignin ^{1}H-^{13}C cross-signals in HSQC spectra of lignin fractions

Label	δC/δH (ppm)	Assignment
-OCH_3	55.6/3.73	C-H in methoxyls
C_β	53.3/3.46	C_β-H_β in phenylcoumarane substructures (C)
B_β	53.3/3.46	C_β-H_β in resinol substructures (B)
A_γ	59.5-59.7/3.40-3.63	Cγ-Hγ in β-O-4’ substructures (A)
I_γ	61.4/4.10	C_γ-H_γ in p-hydroxycinnamyl alcohol end groups (I)
C_γ	62.5/3.73	C_γ-H_γ in phenylcoumaran substructures (C)
B_γ	71.0/3.82-4.18	C_γ-H_γ in resinol substructures (B)
$(A', A'')_\alpha$	71.8/4.86	C_α-H_α in β-O-4’ substructures (A) and γ-acylated β-O-4’ substructures (A’ and A’’)
X_2	72.5/3.02	C_2-H_2 in β-D-xylopyranoside (X)
X_3	73.7/3.22	C_3-H_3 in β-D-xylopyranoside (X)
$BE_{1\alpha}$	81.3/4.65	C_α-H_α in benzyl ether lignin-carbohydrate complex structures
F_β	83.1/5.21	C_β-H_β in oxidized (C_α=O) β-O-4′ substructures (F)
B_α	84.8/4.65	C_α-H_α in resinol substructures (B)
$A_{\beta(S)}$	86.0/4.35	C_β-H_β in β-O-4′ substructures linked to S units (A)
C_α	86.8/5.46	C_α-H_α in phenylcoumaran substructures (C)
$\alpha X_{1(R)}$	92.2/4.88	C_1-H_1 in (1→4)-α-D-xylopyranoside (R)
$\beta X_{1(R)}$	97.4/4.26	C_1-H_1 in (1→4)-β-D-xylopyranoside (R)
$X23_1$	98.9/4.71	C_1-H_1 in 2,3-O-acetyl-β-D-xylopyranoside (X)
$X2_1$	99.4/4.52	C_1-H_1 in 2-O-acetyl-β-D-xylopyranoside (X)
$S_{2,6}$	103.8/6.71	$C_{2,6}$-$H_{2,6}$ in etherified syringyl units (S)
$S'_{2,6}$	106.2/7.23 and 7.07	$C_{2,6}$-$H_{2,6}$ in oxidized (C α=O) syringyl units (S′)
G_2	110.9/6.98	C_2-H_2 in guaiacyl units (G)
G'_2	111.4/7.51	C_2-H_2 in oxidized (C α=O) guaiacyl units (G′)
G_5	114.9/6.77	C_5-H_5 in guaiacyl units (G)
$H_{3,5}$	114.9/6.77	$C_{3,5}$-$H_{3,5}$ in p-hydroxyphenyl units (H)
G_6	119.0/6.80	C_6-H_6 in guaiacyl units (G)

$H_{2,6}$	127.9/7.19	$C_{2,6}$-$H_{2,6}$ in p-hydroxyphenyl units (H)

Table S2. General properties of walnut shell organosolv lignin (WSL)

	M_n（g/moL）	M_w（g/moL）	M_w/M_n	β-O-4: β-β': β-5	G:S:H
WSL	4083	4732	1.16	0.90:0.07:0.03	0.31:0.49:0.2

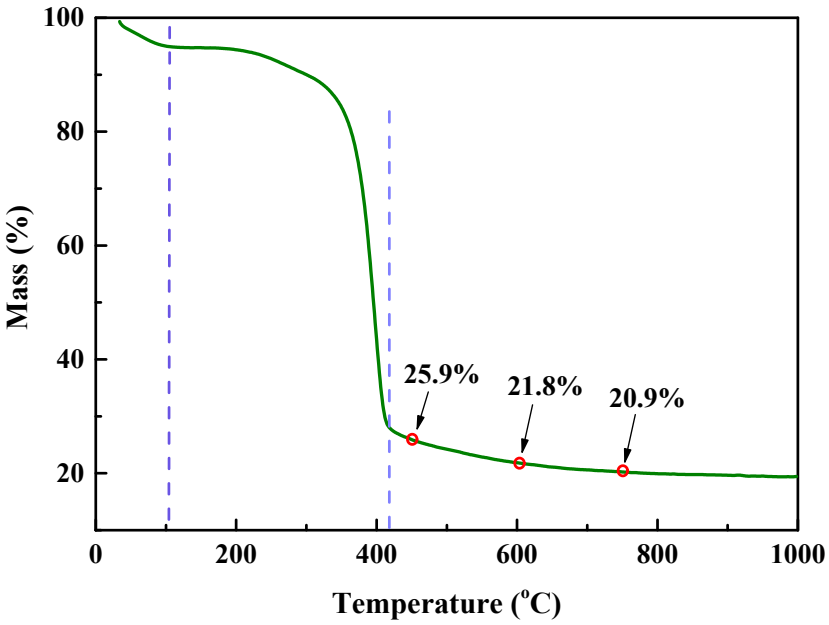

Figure S2. Thermal gravimetric analysis of lignin-F127-Ni polymer.

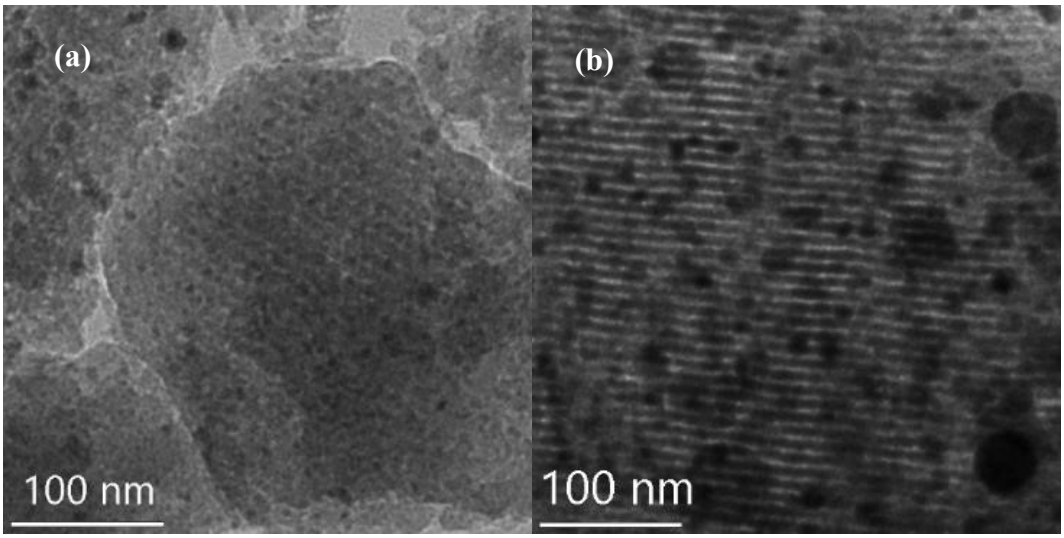

Figure S3. TEM images of OMCs synthesized at 600 ^{o}C from WSL precursor in presence of Ni additives: (a) 0.1 g of $Ni(NO_3)_2 \cdot 6H_2O$ and (b) 0.5 g of $Ni(NO_3)_2 \cdot 6H_2O$.

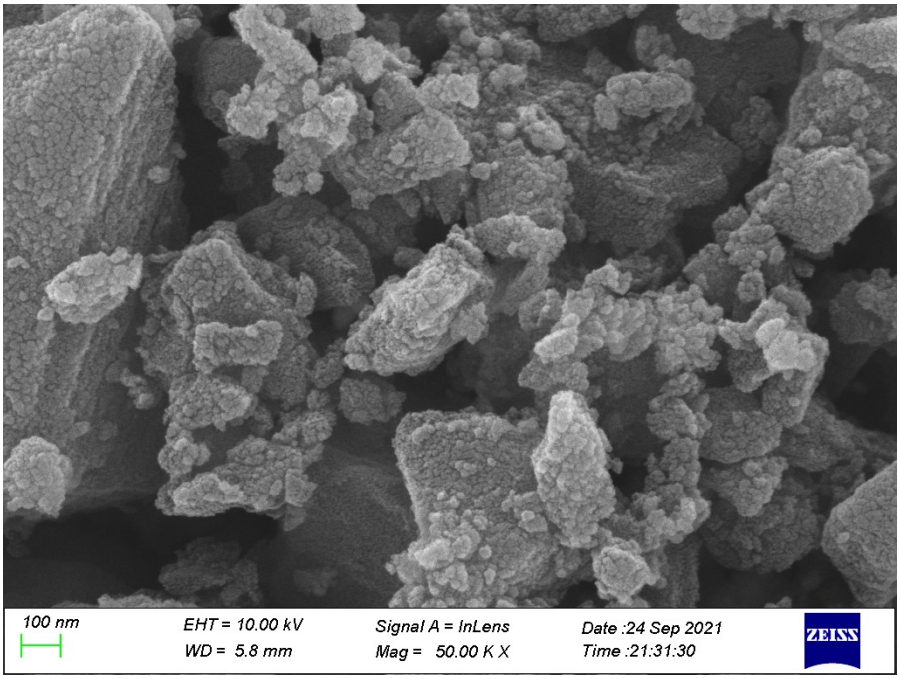

Figure S4. SEM image of Ni@OMC#600.

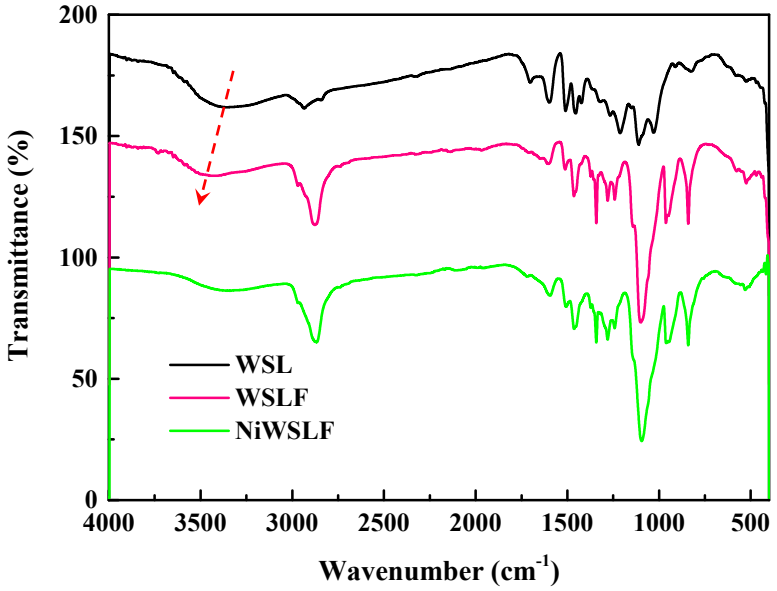

Figure S5. FTIR spectra of organosolv lignin walnut shell (WSL), lignin-F127 composite (WSLF), and lignin-F127-Ni polymer (NiWSLF).

M

Table S3. Catalytic hydrogenation of furfural to tetrahydrofurfuryl alcohol with different catalysts

Catalyst	T (°C)	H_2 pressure (MPa)	Solvent	Conversion (%)	Yield (%)	Ref
Ni#OMC	180	3	2-propanol	100	100	This work
Pd−Ir/SiO_2	2	8	H_2O	>99	94	3
Pd(10 wt%)/Al_2O_3	25	6	2-propanol	80.3	78.2	4
Ru−MoOx/CN	100	2	H_2O	92.1	91.2	5
Rh/C	30	1	H_2O	100	92	6
10%Ni/CNT	130	4	ethanol	99.1	84.3	7
Cu-Ni/CNT	130	4	ethanol	100	90.3	7
Ni-Co-MS	200	8	2-propanol	100	93	8

Recyclability of Ni#OMC-600 used for catalytic hydrogenation

The catalyst could be easily separated from the reaction mixture with a magnet, due to the intrinsic paramagnetism of Ni in the catalyst. After washing with water and ethanol and drying, the separated catalyst was reused for next run. The recycled catalyst afforded a THFA yield of 91% with 8% FAL yield in the second run, and a THFA yield of 82% with 7% FAL yield was constant in value after four recycles, implying good stability of the Ni#OMC-600 material for the catalytic hydrogenation of furfural in the reaction system (Figure S6).

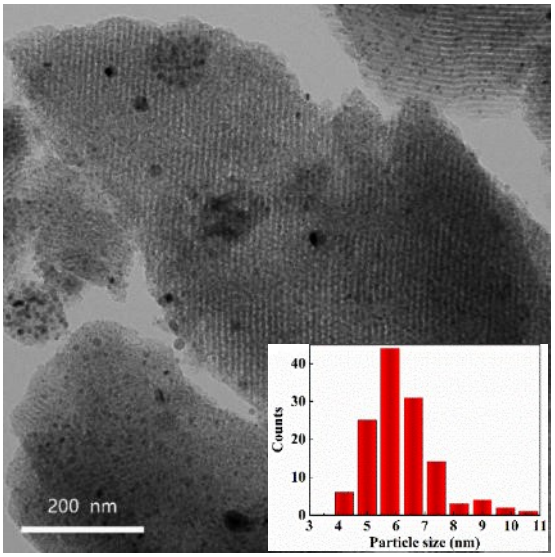

Figure S6. TEM image and Ni particle size distribution of Ni#OMC-600 after four recycles

Catalytic experiments with Ni#OMC

Catalytic hydrogenation of levulinic acid (LA) to γ-valerolactone (GVL)

Hydrogenation reactions were carried out in a closed 30 mL Teflon-lined stainless steel autoclave. In the procedure for hydrogenation of levulinic acid (LA) to γ-valerolactone (GVL), 0.1g catalyst, 0.1 g LA and 10 mL 2-propanol solvent were loaded into the autoclave, which was then closed and purged with 0.5 MPa H_2 for 5 times to remove air. After that, the autoclave was loaded with 3 MPa H_2 and heated to 160 ^oC with continuous stirring at 1000 rpm for the given reaction time. At a given time, the autoclave was rapidly cooled by flowing cold water over it to terminate the reaction, and the reaction mixture was separated by filtration. The resulting liquid solution was analyzed with gas chromatography (Shimadzu-2010) equipped with a Rtx-1 column (30 m × 0.25 mm × 0.25 μm) and an FID detector. Analysis conditions were as follows: N_2 carrier gas, initial column temperature, 120 ^oC that was raised to 180 ^oC at a heating rate of 10 ^oC/min, followed by raising the temperature to 250 ^oC at a heating rate of 20 ^oC/min. Detector temperature was 300 ^oC, and the temperature of gasification chamber was 260 ^oC.

Catalytic hydrogenation of glucose (Glu) to sorbitol (Sorb)

For the catalytic hydrogenation of glucose (Glu) to sorbitol (Sorb) by Ni#OMC sample, a mixture of 0.05 g glucose, 0.05 g catalyst and 5 mL of H_2O were loaded into the stainless-steel reactor, following with the same H_2 purge steps as described above. After that, the reactor was heated to 150 ^oC and kept for 3 h at that temperature. Then, the reactor was quickly cooled with a flowing cold water to terminate the reaction and the reaction mixture was separated by filtration. The collected liquid portion was analyzed by ultraperformance liquid chromatography (Waters Acquity UPLC H-Class) equipped with a refractive index (RI) detector and a sugar column

(SHODEX SH1011). The temperatures of the RI detector and sugar column were set as 35 °C and 50 °C, respectively. H_2SO_4 (5 mM) aqueous solution at a flow rate of 0.5 mL/min was used as the mobile phase.

Table S4. Catalytic conversion of Ni#OMC-600 for the hydrogenation of levulinic acid (LA) to γ-valerolactone (GVL) in 2-propanol and glucose (Glu) to sorbitol (Sorb) in water

Hydrogenation reaction	Temp (°C)	Time (h)	Conversion (%)	Yield (%)	Selectivity (%)
LA-GVL [a]	160	4	100	99.9	99.9
Glu-Sorb [b]	150	3	100	76	76

[a] Reaction conditions: Ni#OMC-600 0.1 g, LA 0.1 g, 2-propanol 10 ml, 3 MPa initial H_2 pressure.

[b] Reaction conditions: Ni#OMC-600 0.05 g, glucose 0.05 g, H_2O 5 ml, 3 MPa initial H_2 pressure.

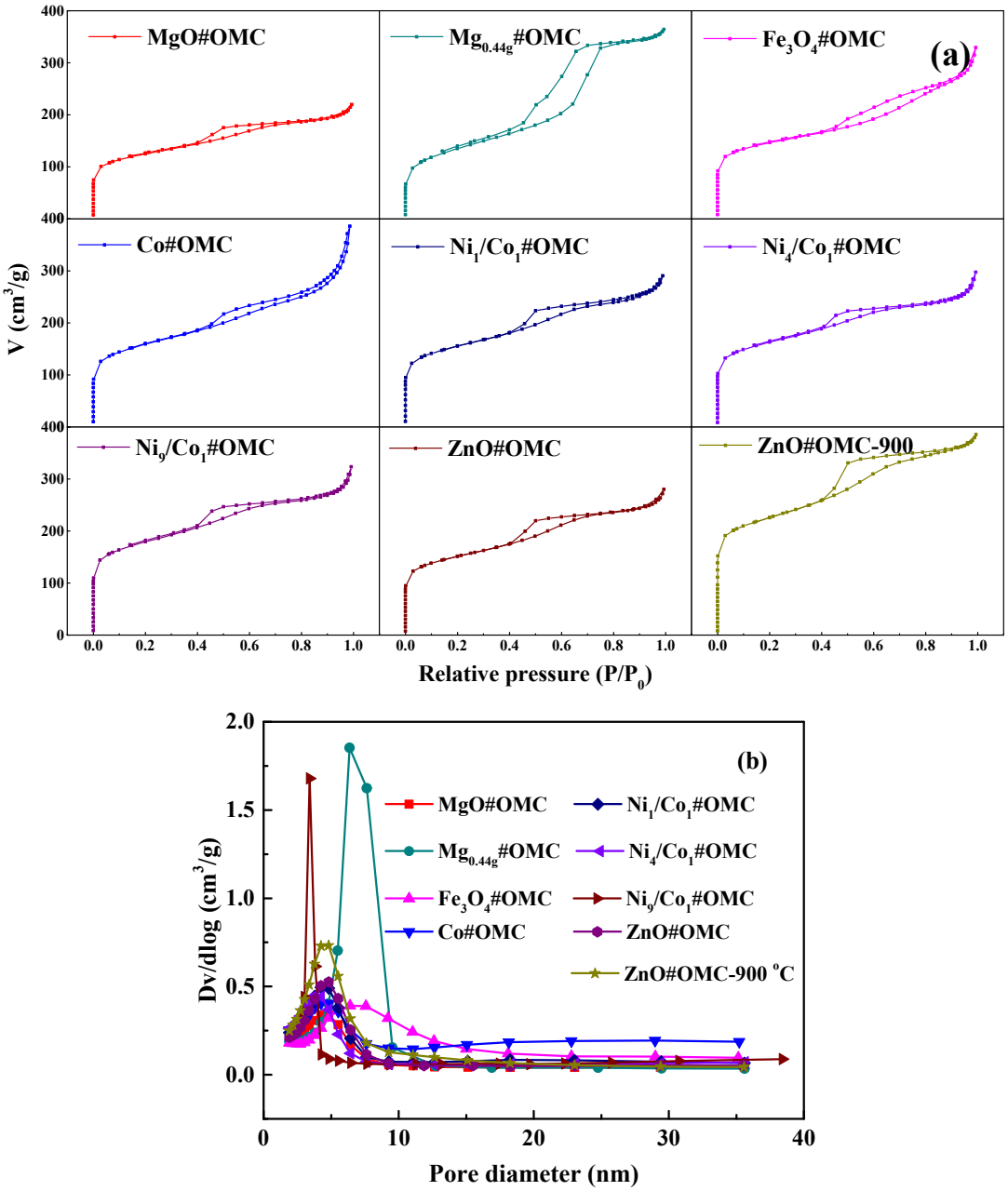

Figure S7. Adsorption characteristics of OMC materials: (a) N_2 adsorption–desorption isotherms, and (b) pore size distribution curves

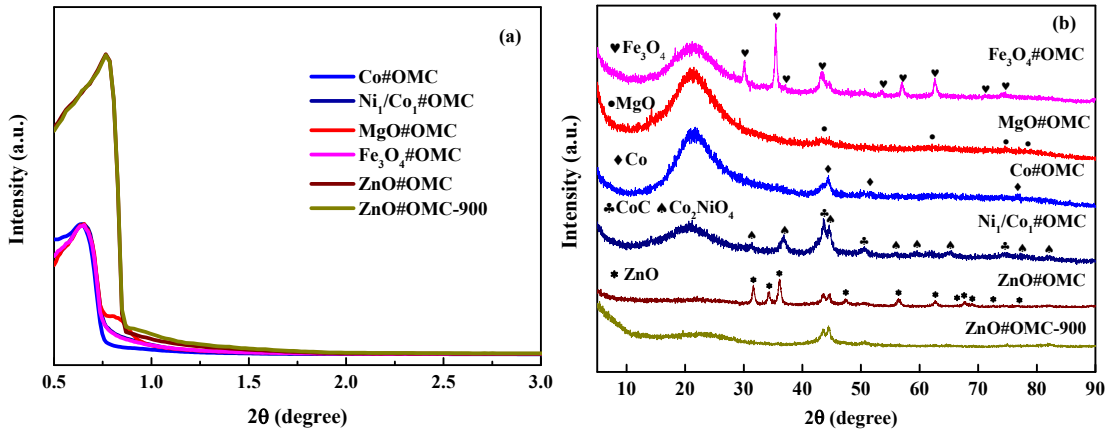

Figure S8. X-ray diffraction (XRD) analyses of OMCs synthesized by metal linkers: (a) low angle XRD and (b) wide angle XRD

Catalytic isomerization of glucose to fructose by $MgO_{0.44}$#OMC

In the isomerization of glucose to fructose experiments, 30 mg catalyst and 5 mL glucose aqueous solution (5 wt%) were added into a 20 mL Teflon-lined stainless steel autoclave, which was closed and purged with 0.5 MPa N_2 for 5 times, and then a pressure of 1 MPa N_2 was used to minimize possible oxidation reactions. The closed autoclave reactor was heated to the specific temperature (80 °C to 120 °C) under conditions of continuous stirring at 1000 rpm for the given time. After reaction was complete, the catalyst was separated from the reaction mixture by centrifugation and the liquid supernatant was analyzed by Ultraperformance Liquid Chromatography (Waters Acquity UPLC H-Class) equipped with a refractive index (RI) detector and a sugar column (SHODEX SH1011). Temperatures of the RI detector and sugar column were set as 35 °C and 50 °C, respectively. The mobile phase was H_2SO_4 aqueous solution (5 mM) that had a flow rate of 0.5 mL/min.

Conversion of glucose and yield of fructose were calculated as follows:

$$Glucose\ conversion = \frac{mole\ of\ \ reacted\ glucose}{mole\ of\ initial\ glucose} \times 100\% \quad \text{(S1)}$$

$$Fructose\ yield = \frac{mole\ of\ produced\ fructose}{mole\ of\ initial\ glucose} \times 100\% \quad \text{(S2)}$$

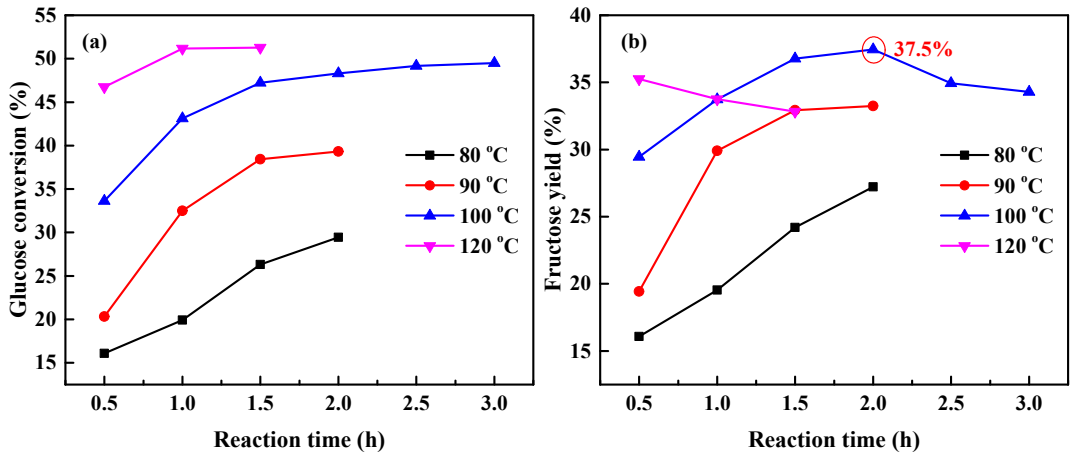

Figure S9. Glucose conversion, fructose yield obtained from catalytic isomerization of glucose over $MgO_{0.44}$#OMC catalyst at 80 °C to 120 °C (Reaction conditions: $MgO_{0.44}$#OMC, 30 mg; 5% glucose 5 mL, 1 MPa N_2)

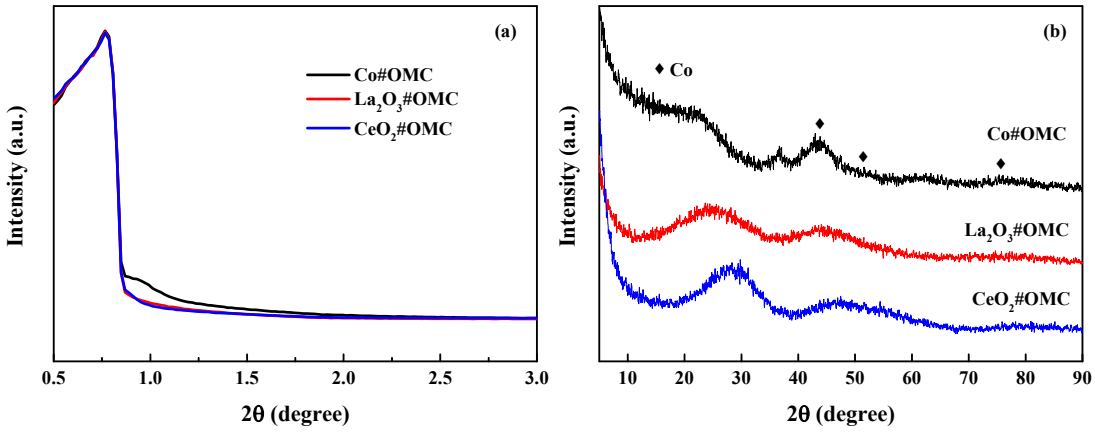

Figure S10. (a) Small and (b) wide angle X-ray diffraction (XRD) patterns of Co#OMC synthesized from macadamia nut shell lignin, La_2O_3#OMC and CeO_2#OMC from tobacco stem lignin

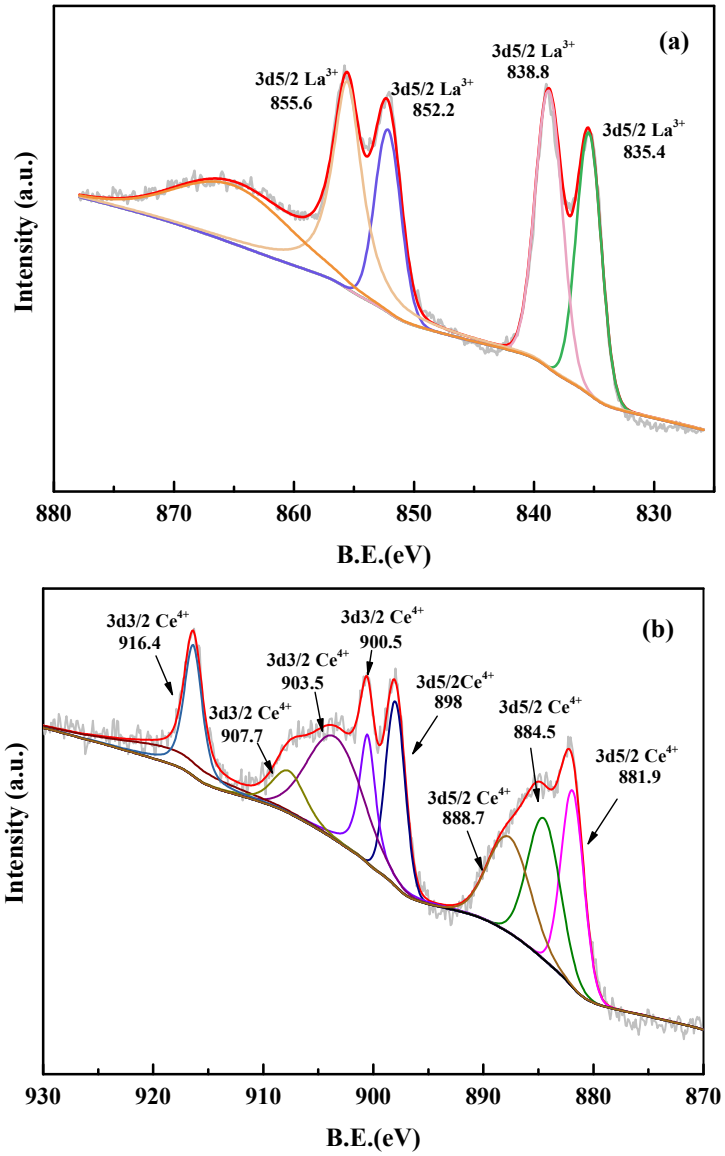

Figure S11. XPS spectra of (a) La_2O_3#OMC and (b) CeO_2#OMC prepared using lignin from tobacco stem

References:

1. S. Yang, T.-Q. Yuan and R.-C. Sun, *ACS Sustainable Chem. Eng.*, 2016, **4**, 1006-1015.
2. P. J. Deuss, M. Scott, F. Tran, N. J. Westwood, J. G. de Vries and K. Barta, *J. Am. Chem. Soc.*, 2015, **137**, 7456-7467.
3. Y. Nakagawa, K. Takada, M. Tamura and K. Tomishige, *ACS Catalysis*, 2014, **4**, 2718-2726.
4. S. Bhogeswararao and D. Srinivas, *J. Catal.*, 2015, **327**, 65-77.
5. Y. Cao, H. Zhang, K. Liu, Q. Zhang and K.-J. Chen, *ACS Sustainable Chem. Eng*, 2019, **7**, 12858-12866.
6. B. M. Matsagar, C.-Y. Hsu, S. S. Chen, T. Ahamad, S. M. Alshehri, D. C. W. Tsang and K. C. W. Wu, *Sustainable Energy Fuels*, 2020, **4**, 293-301.
7. L. Liu, H. Lou and M. Chen, *Int. J. Hydrogen Energy*, 2016, **41**, 14721-14731.
8. J. Parikh, S. Srivastava and G. C. Jadeja, *Ind. Eng. Chem. Res.*, 2019, **58**, 16138-16152.